Density Matrix Analysis, Simulation, and Measurements of Electronic Absorption and Fluorescence Spectra of Spirobifluorenes

Vladimir Lukeš,*,† Tibor Pálszegi,† Franz Milota,‡ Jaroslaw Sperling,‡ and Harald Friedrich Kauffmann‡

Department of Chemical Physics, Slovak University of Technology, Radlinského 9 SK-812 37 Bratislava, Slovakia, and Institute of Physical Chemistry, University of Vienna, Währingerstrasse 42, A-1090 Vienna, Austria

Received: August 11, 2005; In Final Form: December 3, 2005

The linear absorption and fluorescence spectra as well as the oscillator strengths of 2,2′,7,7′-tetraphenyl-9,9′-spirobifluorene (**A**), 2,2′,7,7′-tetrakis(biphenyl-4-yl)-9,9′-spirobifluorene (**B**), and 2,2′,7,7′-tetrakis(9,9′-spirobifluoren-2-yl)-9,9′-spirobifluorene (**C**) are calculated on the basis of the collective electronic oscillator (CEO) approach of Mukamel et al. (see, e.g., *Chem. Rev.* **2002**, *102*, 3171). The graphical visualization and quantitative characterization of CEO modes allows one to extract the real-space distribution of electronic excitations of the molecules under study. Effects of the lengthening and branching of the oligophenylene segments have been analyzed. The influence of the lowest excited (S_1) vs ground-state (S_0) geometry changes on the CEO modes is investigated and related to the geometry changes of the molecular parts. The obtained theoretical results are in good agreement with experimental trends observed in absorption and fluorescence data.

1. Introduction

π-conjugated organic molecules with suitable optical nonlinearities and spectral characteristics occupy a prominent position in modern research because of their high cost-effectiveness, low dielectric constants, fast nonlinear optical response, and easy integration into passive and active devices.[1−7] A fascinating and promising class of conjugated molecules are oligophenylenes with spiro-linkage architecture. The branches of such (spiro-)molecules are connected by a common sp^3-carbon, the so-called spiro-center. By connection of various oligophenylenic segments through spiro-linkages, supramolecules of spiro- and π-conjugated constituents can be designed. The spiro-linkage between the perpendicularly oriented π-conjugated segments improves the processability and the morphologic stability. These systems are characterized by a tunable balance between rigidity and rotational (torsional) freedom. The rigidity suppresses nonradiative deactivation pathways (leading to high photoluminiscence quantum yields) and increases the effective π-electron conjugation. On the contrary, the remaining rotational degrees of freedom keep Stokes shifts large, due to geometrical relaxation (following electronic redistribution) of the lowest excited singlet state. [8−11]

Identifying the relation between electronic excitation properties and the chemical as well as the geometrical structure of molecules is the key tool for a directed design of new electronic compounds and tuning of their photoelectronic properties.[12,13] The synthesis, preparation, and optical and basic theoretical characterization of spiro-linked materials have been presented recently in several works.[14−23] Johanson et al.[16] studied 2,2′,7,7′-tetrakis(biphenyl-4-yl)-9,9′-spirobifluorene and 2,2′-bis(5-(4-*tert*-butylphenyl)-1,3,4-oxadiazol-2-yl)-9,9′-spirobifluorene theoretically, focusing calculations on the lowest-energy optical transitions. The electron-vibrational dynamics of photoexcited polyfluorenes with a single spiro-linkage was studied at the semiempirical level by Franco and Tretiak.[24] In this paper we present the theoretical and experimental study of 2,2′,7,7′-tetraphenyl-9,9′-spirobifluorene (**A**), 2,2′,7,7′-tetrakis(biphenyl-4-yl)-9,9′-spirobifluorene (**B**), and 2,2′,7,7′-tetrakis(9,9′-spirobifluoren-2-yl)-9,9′-spirobifluorene (**C**) (see Figure 1). Considering the size of the oligomers to be treated in this work, we use a density functional (DFT) approach for the calculation of optimized electronic ground-state geometries and its time-dependent (TD) extension for excited-state geometries in the first step. Using these geometries, the calculation and analysis of quantitites related to electronic linear absorption and stationary fluorescence, i.e. spectral line energies and oscillator strengths, are realized using the collective electronic oscillator (CEO) method of Mukamel et al.[25−29] We are interested in the analysis of the effect of lengthening of the oligophenylene segments with and without increasing the number of spiro-linkages (i.e., molecule **B** vs **A** and **C** vs **A**, **B**). We study how electronic delocalization in dominant excited states is affected by segmental lengths and peripheral spiro-linkages. We further analyze the electronic localization and charge-transfer effects induced by peripheral spiro-linked oligophenylene segments. The calculated optical quantities will be compared with experimental measurements obtained in solution and bulk material.

2. Methodology

2.1. CEO Method. The CEO calculation starts with the determination of the Hartree−Fock ground-state one-electron density matrix $\bar{\rho}$ using a suitable Hamiltonian (here, as in most cases, determined by the ZINDO/S approach[30]). The diagonal elements of $\bar{\rho}$ represent the electronic charge density at the atoms whereas the off-diagonal elements reveal the bonding structure associated with each pair of atoms (i.e., bond order). When the

† Slovak University of Technology.
‡ University of Vienna.
* Corresponding author. E-mail: vladimir.lukes@stuba.sk.

10.1021/jp054507d CCC: $33.50
Published on Web 01/17/2006

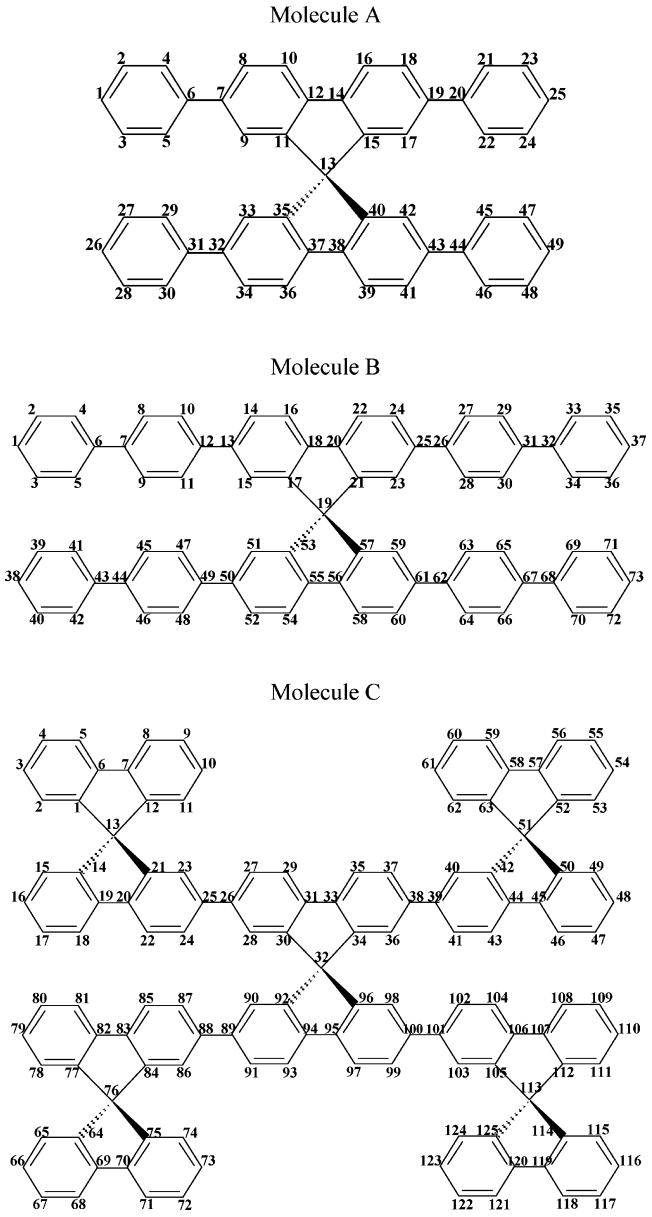

Figure 1. Chemical structure and numbering of carbon atoms for a) 2,2′,7,7′-tetraphenyl-9,9′-spirobifluorene (molecule **A**), (b) 2,2′,7,7′-tetrakis(biphenyl-4-yl)-9,9′-spirobifluorene (molecule **B**), and (c) 2,2′,7,7′-tetrakis(9,9′-spirobifluoren-2-yl)-9,9′-spirobifluorene (molecule **C**).

molecule interacts with an external driving field, its electronic density matrix acquires a time-dependent component $\delta\rho(t)$, which can be expanded as

$$\delta\rho(t) = \sum_{\nu}[a_{\nu}(t)\xi_{\nu} + a^{*}_{\nu}(t)\xi_{\nu}^{+}] \tag{1}$$

where $a_{\nu}(t)$ are time-dependent expansion coefficients and the electronic normal modes ξ_{ν} represent the optical transition between the ground $|g\rangle$ and electronically excited states $|\nu\rangle$. The one-electron transition density matrix eigenmodes ξ_{ν} are formed by matrix elements of the real space (atomic orbital based) electron−hole (e−h) operator $\hat{c}_m^{+}\hat{c}_n$, as follows:

$$(\xi_{\nu})_{mn} = \langle\nu|\hat{c}_m^{+}\hat{c}_n|g\rangle \tag{2}$$

The CEO modes can be obtained as the eigenmodes of the linearized time-dependent Hartree−Fock equations of motion for the time-dependent density matrix driven by the external field, totally bypassing the calculation of many-electron eigenstates. These modes describe collective motions of electrons and holes and carry substantially less information than the many-electron eigenstates but more than required for calculating spectroscopic observables. The eigenfrequencies Ω_{ν} of CEO modes provide the optical transition frequencies. The oscillator strength of the g to ν transition is given by

$$f_{\nu} = 2\Omega_{\nu}[\mathrm{Tr}(\mu\xi_{\nu})]^2 \tag{3}$$

where μ is the dipole moment operator.[25−28] Because the relevant optical excitations studied here are of $\pi-\pi^*$ type, we focus our analysis on the π-part of the transition density matrices. Their size is determined by the number of carbon atoms, labeled according to Figure 1. The two-dimensional representation of the CEO eigenmodes allows a visual inspection of the electronic redistribution (in real space) induced by optical excitation, and its quantitative specification. The diagonal elements $(\xi_{\nu})_{nn}$ give the excess charge created at the nth atom by the transition to the νth electronic state. The off-diagonal elements $(\xi_{\nu})_{nm}$, also known as electronic coherences, represent the joint probability amplitude of creating an excess hole at atom n (x-axis) and an electron at atom m (y-axis). The coherences control the scaling of optical properties with molecular size and give information over which distance atoms can communicate. The extent and enlargement of electronic coherences (and CEO modes) directly reflects the localization of an exciton created by optical excitation.

For a quantitative measure of the spatial distribution of induced electronic (transition) charge densities and coherences (dynamic bond-orders), the diagonal length L_{d} and the coherence size L_{c} of the CEO modes have been defined.[25] The diagonal length L_{d} describes the number of atoms over which the optical excitation is spread and is given by

$$L_{\mathrm{d}} \equiv \left[\sum_{n}\left(\frac{|\xi_{nn}|}{\sum_{j}|\xi_{jj}|}\right)^2\right]^{-1} \tag{4}$$

The coherence size L_{c} represents the degree of coherence and (similar to the diagonal length) indicates the electronic delocalization (transfer) distances from ground-state electronic locations. It is defined in terms of the coherence participation ratio

$$L_{\mathrm{c}} \equiv \left[L_{\mathrm{d}}\sum_{mn}\left(\frac{|\xi_{nm}|}{\sum_{ij}|\xi_{ij}|}\right)^2\right]^{-1} \tag{5}$$

To characterize intra- and inter-chromophore electron exchange, the probabilities for the electron and the hole to be on different chromophores (charge transfer), p_{12} and p_{21}, can be defined.[25] These quantities are given by

$$p_{ij} = \sum_{n_i,m_j}[(\xi_{\nu})_{n_i m_j}]^2 \tag{6}$$

where n_i and m_j are indices of atomic orbitals of chromophoric segments i and j, respectively. Different values for p_{12} and p_{21} in a chromophore pair (formed, e.g., by two chromophores or two parts of a molecule) indicate global charge transfer. For $p_{21} = p_{12}$, inter-chromophore delocalization results in spatially charged excited states.

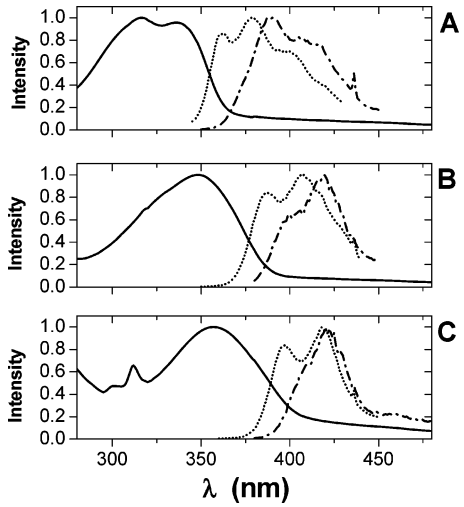

Figure 2. Experimental absorption (solid line for CH_2Cl_2 solution) and fluorescence spectra (dashed line for CH_2Cl_2 solution and dotted line for bulk) of molecules **A**, **B**, and **C**.

2.2. Calculation Details. Ground- and lowest singlet excited-state geometries are optimized at the DFT level and the TDDFT level, respectively, using the B3LYP functional. Because of the large geometrical variability of the studied molecules, we restrict our study to the conformations with the lowest total energy identified using the AM1 method.[23] On the basis of the optimized geometries, the electronic absorption and luminescence spectra and one-electron ground state and transition density matrices have been calculated by the CEO method. Vertical excitations are computed at the ground-state geometry. The fluorescence transition is obtained as the vertical deexcitation of the geometrically optimized excited state. Carbon atoms of individual phenyl units and of different oligophenylene segments (branches) are numbered consecutively (cf. Figure 1). We used a semiempirical ZINDO/S Hamiltonian with $\sigma-\sigma$ and $\pi-\pi$ overlap weighting factors of 1.267 and 0.625, respectively. The value of 0.625 obtained by the CEO method reproduces the wavelength of maximal absorption of spiro-bifluorene (308 nm, measured in solution) quite satisfactorily. [31] The split-valence (SV) basis sets have been used. All calculations were done using the Turbomole[32] and CEO-ZINDO/S program packages.[33]

2.3. Instrumentation. Absorption spectra were recorded on a Perkin-Elmer Lambda spectrometer in a 10 mm quartz cuvette. All used solvents were spectroscopic grade quality (UVASOL from Merck). Emission spectra were recorded with a double-grating monochromator and photomultiplier tube in a 10 mm quartz cuvette (CH_2Cl_2 solution) or on Suprasil substrates (bulk). Excitation energies were tuned into the long wavelength band of the respective absorption spectra (335−360 nm). Bulk samples were produced by spin-coating from CH_2Cl_2 solution (5 mg/20 mL) at room temperature. All measurements were carried out at room temperature (298 K).

3. Results and Discussion

The experimental absorption spectrum of compound **A** is characterized by two peaks, centered at approximately 317 and 336 nm (see Figure 2). In the cases of **B** and **C**, the absorption spectra are characterized by a single broad and unstructured band. No vibrational structure is observed. This is attributed to rotational freedom of the phenyl groups in the electronic ground state. In contrast to the absorption spectra, the positions of the experimental fluorescence maxima reveal a larger interval of values (from 363 to 440 nm) with some vibrational structure (see Table 1 and Figure 2). Three different maxima are clearly identified. Molecule **A** shows the smallest Stokes shift in solution (2214 cm^{-1}) due to small geometric differences between the electronic ground- and excited-states. The increasing number of nonhindered inter-ring torsional angles (molecule **B**) leads to a larger value of the Stokes shift (2979 cm^{-1}). Molecule **C** has an approximately 200 cm^{-1} smaller Stokes shift in comparison to **B**, probably due to the reduction of nonhindered inter-ring torsional angles. The measured averaged fluorescence lifetimes decrease with the size of the molecule (see the data **B**, **C** vs **A** in Table 1).

The optimized structures obtained from the DFT calculations indicate a propeller shape because the branches of spiro-systems are mutually perpendicular. This perpendicularity is preserved for any type of conformation in the electronic ground state and the lowest excited singlet state. The mutual orientation of the phenyl rings in molecule **A** substituted at the central spiro-bifluorene and of the nearest-neighbor rings bonded to them is 37° in the ground-state geometry. In the case of molecule **B**, the inner dihedral angles are lower by about 2° than the outer ones which are 35°. The mutual (torsional) angles between the spiro-bifluorene fragments in molecule **C** are 37°. This last value agrees very well with the experimental value of 36° obtained for the α-type *p*-fluorene oligomer.[34] The elongation of the molecular chain (from **A** to **B**) leads to small changes in the inter-ring distances (see Table 2).

The vertical electronic excitation of the studied molecules into the lowest electronic singlet excited state (S_1) is followed by the relaxation of the molecular geometry of the first or second molecular fragment to higher planarity. The optimal TDDFT torsional angles between neighboring pairs of phenyl rings (both not being involved in the spiro-bifluorene) are found to be smaller in the singlet excited state (23° for **A**, outer dihedral angles of 25° and inner angles of 14° for **B** and 16° for **C**). The bonds between the aromatic rings in the central-spiro linkage are shortened while the neighboring bonds are elongated. This leads to formation of a quinoide-type structure. The $C-CH_2$ bond lengths are not affected by increasing the molecular size and by electronic excitation (the values are ca. 1.541 Å). This indicates that these bonds are not part of the π-conjugated system.

The calculated Ω_v eigenvalues of the CEO modes correspond to vertical excitation energies from the ground-state geometry; their values are collected in Table 3. The calculated absorption wavelengths are in the range between 340 and 359 nm. The CEO modes with nonnegligible oscillator strengths are characterized by two double-degenerate peaks as a consequence of the symmetric structure of the studied systems and negligible trapping between the monomer chains. In other words, the resulting excited states are completely delocalized between both segments forming a so-called Frenkel exciton.[24] Planarization of distinct fragments (subsequent to optical excitation) leads to a red shift in energies. The CEO fluorescence wavelengths corresponding to the lowest singlet excited-state geometry are in the interval from 380 to 418 nm (see Table 2). Considering the fact that experimental spectra are subject to a Boltzmann distribution of conformations, the theoretical data agree quite well with the measurements (see Table 1).

On the basis of fluorescence energies and oscillator strengths, radiative lifetimes have been computed using the Einstein transition probability according to the formula (in au)[35]

$$\tau = \frac{c^3}{2(E_{\mathrm{Flu}})^2 f} \qquad (7)$$

TABLE 1: Experimental Spectral Characteristics of the Compounds under Study

molecule	medium	λ_{abs}[a] (nm)	λ_{exc}[b] (nm)	λ_{fluor}[c] (nm)	$\bar{\tau}$[d] (ps)	$\Delta\upsilon_{ST}$[e] (cm^{-1})
A	CH_2Cl_2	317, 336	336	363, 378, 399	1124	2214
	bulk	337	337	390, 405, 416	450−800	4033
B	CH_2Cl_2	347	344	387, 408	785	2979
	bulk	347	347	402, 419	390−470	3943
	bulk	346[f]				
C	CH_2Cl_2	357, 301	355	396, 418,440	831	2759
	bulk	360	360	409, 420	380−450	3328
	bulk	353, 310[f]				

[a] Absorption maxima. [b] Excitation wavelengths. [c] Fluorescence maxima. [d] Averaged fluorescence lifetimes. [e] Stokes shift between maxima of absorption and fluorescence bands. [f] Data taken from ref 22.

TABLE 2: Calculated Optimal Distances (in Å) and DFT/TDDFT Total Energies E_{tot} (in E_h) of the Compounds under Study in the Electronic Ground (GS) and the Lowest Excited (ES) States

	molecule **A**			molecule **B**			molecule **C**	
distance/E_{tot}	GS −1883.540791	ES −1883.416548	distance/E_{tot}	GS −2806.292417	ES −2806.175845	distance/E_{tot}	GS −4799.224498	ES −4799.111104
d_{2-3} (d_{23-24})	2.428 (2.428)	2.427 (2.427)	d_{2-3} (d_{35-36})	2.427 (2.427)	2.427 (2.427)	d_{2-4} (d_{60-62})	2.447 (2.447)	2.447 (2.447)
d_{4-5} (d_{21-22})	2.427 (2.427)	2.427 (2.427)	d_{4-5} (d_{33-34})	2.426 (2.426)	2.427 (2.427)	d_{1-5} (d_{63-59})	2.449 (2.447)	2.449 (2.449)
d_{6-7} (d_{19-20})	1.491 (1.491)	1.491 (1.491)	d_{6-7} (d_{31-32})	1.490 (1.490)	1.490 (1.490)	d_{6-7} (d_{58-57})	1.476 (1.476)	1.476 (1.476)
d_{8-9} (d_{17-18})	2.437 (2.437)	2.437 (2.437)	d_{8-9} (d_{29-30})	2.417 (2.417)	2.417 (2.417)	d_{8-12} (d_{52-56})	2.449 (2.449)	2.449 (2.449)
d_{10-11} (d_{16-15})	2.440 (2.440)	2.440 (2.440)	d_{10-11} (d_{27-28})	2.418 (2.418)	2.418 (2.418)	d_{9-11} (d_{53-55})	2.447 (2.447)	2.447 (2.447)
d_{12-14}	1.472	1.472	d_{12-13} (d_{25-26})	1.489 (1.489)	1.489 (1.489)	d_{15-17} (d_{47-49})	2.448 (2.448)	2.448 (2.448)
			d_{14-15} (d_{23-24})	2.437 (2.437)	2.438 (2.438)	d_{14-18} (d_{46-50})	2.450 (2.450)	2.450 (2.450)
d_{27-28} (d_{47-48})	2.428 (2.428)	2.428 (2.428)	d_{16-17} (d_{21-22})	2.440 (2.440)	2.441 (2.441)	d_{19-20} (d_{44-45})	1.474 (1.474)	1.474 (1.474)
d_{29-30} (d_{45-46})	2.427 (2.427)	2.431 (2.431)	d_{18-20}	1.472	1.471	d_{21-22} (d_{42-43})	2.440 (2.440)	2.442 (2.442)
d_{31-32} (d_{43-44})	1.491 (1.491)	1.474 (1.474)				d_{23-24} (d_{40-41})	2.438 (2.438)	2.439 (2.439)
d_{33-34} (d_{41-42})	2.437 (2.437)	2.451 (2.451)	d_{39-40} (d_{71-72})	2.427 (2.427)	2.427 (2.427)	d_{25-26} (d_{38-39})	1.490 (1.490)	1.489 (1.489)
d_{35-36} (d_{39-40})	2.440 (2.440)	2.462 (2.462)	d_{41-42} (d_{69-70})	2.426 (2.426)	2.430 (2.430)	d_{27-28} (d_{36-37})	2.438 (2.438)	2.438 (2.438)
d_{37-38}	1.472	1.438	d_{43-44} (d_{67-68})	1.490 (1.490)	1.476 (1.476)	d_{29-30} (d_{34-35})	2.440 (2.440)	2.443 (2.443)
			d_{45-46} (d_{65-66})	2.417 (2.417)	2.421 (2.421)	d_{31-33}	1.472	1.471
			d_{47-48} (d_{63-64})	2.418 (2.418)	2.427 (2.427)			
			d_{49-50} (d_{61-62})	1.489 (1.489)	1.458 (1.458)	d_{65-67} ($d_{117-115}$)	2.447 (2.447)	2.447 (2.447)
			d_{51-52} (d_{59-60})	2.437 (2.437)	2.458 (2.458)	d_{64-68} ($d_{114-118}$)	2.449 (2.449)	2.449 (2.449)
			d_{53-54} (d_{57-58})	2.440 (2.440)	2.466 (2.466)	d_{69-70} ($d_{119-120}$)	1.476 (1.476)	1.476 (1.476)
			d_{55-56}	1.472	1.430	d_{71-75} ($d_{121-125}$)	2.449 (2.449)	2.449 (2.449)
						d_{72-74} ($d_{122-124}$)	2.447 (2.447)	2.447 (2.447)
						d_{78-80} ($d_{109-111}$)	2.448 (2.448)	2.451 (2.451)
						d_{77-81} ($d_{108-112}$)	2.450 (2.450)	2.456 (2.457)
						d_{82-83} ($d_{106-107}$)	1.474 (1.474)	1.458 (1.458)
						d_{84-85} ($d_{104-105}$)	2.440 (2.440)	2.448 (2.448)
						d_{86-87} ($d_{102-103}$)	2.438 (2.438)	2.452 (2.452)
						d_{88-89} ($d_{100-101}$)	1.490 (1.490)	1.459 (1.459)
						d_{90-91} (d_{98-99})	2.438 (2.438)	2.458 (2.458)
						d_{92-93} (d_{96-97})	2.440 (2.440)	2.466 (2.466)
						d_{94-95}	1.472	1.431

where c is the velocity of light, E_{Flu} is the transition energy, and f is the oscillator strength. The obtained values (1770 ps for **A**, 1196 ps for **B**, and 1333 ps for **C**) are in fairly good agreement with experimental trends (see Table 1).

Panels $\bar{\rho}$ at the top of Figure 3 display the contracted ground-state reduced single-electron density matrices of **A**, **B**, and **C**, respectively, in the ground-state molecular geometry. These matrices are dominated by diagonal and near-diagonal elements, reflecting bonds between nearest neighbors. Individual benzene rings and the spiro-linkage carbon atoms are clearly identified. Partial charges on carbon atoms range from 0.96 to 1.1. Hydrogen bonded carbons show the highest charge magnitude, while spiro-linkage carbons show the lowest one.

The first double degenerate electronic modes ξ_1 and ξ_2 of **A** and **B** indicate excited-state delocalization over the entire molecule with strong coherence, both between phenyls through the spiro-center (inter-branch coherence) and in the individual branches (intra-branch coherence) (see the second and forth rows of Figure 3). The patterns of these CEO modes are nearly symmetric relative to both diagonals—they have nearly the same diagonal and off-diagonal blocks. The ξ_1 and ξ_2 modes of **A** and **B** differ in the diagonal direction delocalization. This corresponds to the difference of probabilities p_{11} and p_{22} for both electron and hole to reside on branch 1 and 2 (values of 0.5 and 0.4 for **A** and 0.6 and 0.4 for **B**—see Table 3). The probabilities p_{ij} have been calculated without including the probability on the spiro-carbon.

The probabilities p_{12} and p_{21} for the electron and the hole to be on different branches are very small, indicating a very small charge transfer. There is only very little delocalization from the end of one branch to the other branch, resulting in the low coherences around the intense off-diagonal blocks. The diagonal length L_d of the ξ_1 mode of **B** is increased by a factor of ~1.38 (corresponding to a value of 34.5 for **A**), while the lengths of the phenylene segments have grown by a factor of 1.5. The coherence length L_c of ξ_1 is less affected by the lengthening of the segments, in molecule **B**, it is approximately 26.7 (23.1 for **A**, compare with Table 2).

The comparison of the CEO modes of the more branched spiro-molecule **C** with the less branched molecules **A** and **B** allows one to investigate how the structure and monomer size affect the excited-state electronic localization. The degenerate CEO modes 1 and 2 are localized only on the first or second main branch and show negligible electron delocalization. While

TABLE 3: CEO-ZINDO/S Absorption (Ω_{abs}) and Fluorescence Energies (Ω_{flu}) and their Corresponding Oscillator Strengths (*f*), the Diagonal Lengths (L_d), Coherence Sizes (L_c) of the CEO Modes, and Probabilities for the Electron and the Hole to Be on the Same (p_{11} and p_{22}), and on Different Branches (p_{12} and p_{21}) of the Respective Molecule

molecule	mode	Ω_{abs} (nm)	f	L_d	L_c	p_{11}	p_{22}	p_{12}	p_{21}	mode	Ω_{flu} (nm)	f	L_d	L_c	p_{11}	p_{22}	p_{12}	p_{21}
A	1	340	1.05	34.5	23.1	0.5	0.4	0.0	0.0	1	378	1.21	19.0	24.1	0.0	1.0	0.0	0.0
	2	340	1.05	34.5	23.1	0.4	0.5	0.0	0.0	2	378	1.21	19.1	24.1	1.0	0.0	0.0	0.0
	13	263	0.40	40.7	28.4	0.3	0.3	0.2	0.2									
	14	263	0.40	40.7	28.4	0.3	0.3	0.2	0.2									
	15	252	0.56	32.2	21.8	0.4	0.4	0.1	0.1									
B	1	351	1.74	47.7	26.7	0.6	0.4	0.0	0.0	1	393	1.93	25.1	28.6	0.0	1.0	0.0	0.0
	2	351	1.74	47.7	26.7	0.4	0.6	0.0	0.0	2	393	1.93	25.1	28.6	1.0	0.0	0.0	0.0
	3	306	0.07	54.3	20.6	0.7	0.3	0.0	0.0									
	7	294	0.08	40.8	16.5	0.5	0.5	0.0	0.0									
	8	294	0.08	40.8	16.5	0.5	0.5	0.0	0.0									
	9	285	0.59	63.8	19.4	0.5	0.5	0.0	0.0									
	10	285	0.59	63.8	19.4	0.5	0.5	0.0	0.0									
C	1	359	1.88	33.0	29.5	0.0	1.0	0.0	0.0	1	418	1.99	31.2	30.8	1.0	0.0	0.0	0.0
	2	359	1.84	33.0	29.6	1.0	0.0	0.0	0.0	2	418	1.99	31.2	30.8	0.0	1.0	0.0	0.0
	5	308	0.18	72.6	24.1	0.8	0.2	0.0	0.0									
	6	308	0.18	72.6	24.1	0.2	0.8	0.0	0.0									
	8	305	0.36	51.9	18.4	0.2	0.8	0.0	0.0									
	9	305	0.36	51.9	18.4	0.8	0.2	0.0	0.0									
	10	305	0.38	49.3	17.9	0.5	0.5	0.0	0.0									

the diagonal length of the ξ_1 mode of **C** (see the third surface plot in the third row of Figure 3) is decreased in comparison to **B** (value of 47.7), as an effect of the peripheral spiro-linkage, the coherence length has increased to 29.5. The phenylene segments of **C** are more planar than the ones of **B**, but the spiro-group connected biphenylenes reduce the excited-state delocalization. The difference in the diagonal blocks of the surface plot of ξ_1 for **C** is large. The probabilities p_{11} (or p_{12}) for both electron and hole to reside on branch 1 (or 2) are 1.0 (see Table 3).

After excitation of an electron to the first excited-state, we observe self-trapping of the excitation on a single chain in molecules **A** and **B**. Structurally, this is reflected as a reduction of the bond length alternation and the dihedral angles as well as strong changes in bond lengths of the central monomer of one chain (the second chain remains nearly unaltered by this process). The plots in the third row in Figure 3 represent the ξ_1* mode in the fluorescing (S_1) excited-state geometry. These distinct changes in each of the chains composing the spiro-system lift the initial degeneracy of the first two excited states. Quantitatively, the probabilities p_{11} and p_{22} for the ξ_1* mode have changed from their above-mentioned ground-state geometry values (see also Table 3) to values of 0.0 and 1.0, respectively. The delocalization length L_d is two times lower than in the electronic ground-state. On the other hand, a small increase in coherence size is indicated.

All the oscillator strengths of the ξ_1, ξ_2, ξ_1*, and ξ_2* CEO modes individually increase with growing molecular weight. The growth for **C** relative to **B** is not so large as the increase for **B** relative to **A** (see Table 3). It follows, that lengthening of a branch has a larger effect on the oscillator strength than an increase of the number of spiro-groups. The oscillator strengths for the electronic excited-state geometry (S_1) are slightly increasing for molecule **A** and **B**, but decreasing for molecule **C**.

Higher CEO modes with nonnegligible oscillator strengths of **A** show different behaviors with respect to coherences. The double degenerate modes ξ_{13} and ξ_{14} show strong inter-branch and weaker intra-branch coherences (see first column in Figure 3). The values of p_{12} and p_{21} are 0.2. For **B**, all double degenerate modes ξ_7, ξ_8 and ξ_9, ξ_{10} (cf. second column of Figure 3) have both small intra- and inter-branch coherences, indicating that a precise description within the excitonic picture would necessitate the inclusion of (inter-branch charge transfer) Wannier exciton contributions.

Diagonal and coherence lengths (L_d and L_c) of the modes described in the previous paragraph give a measure of spatial (de)localization. The values in Table 3 imply that the ξ_{13} and ξ_{14} mode of **A** have the largest coherence length, the largest diagonal length and the largest sum of these quantities, respectively. Overall, the comparison of diagonal and coherence lengths of the CEO modes of **A** and **B** clearly shows that chain lengthening supports delocalization.

In the case of molecule **C**, the delocalization lengths of the double degenerated CEO modes ξ_5 and ξ_6 are much larger than the one of mode ξ_1 (cf. third column of Figure 3). This follows from the fact that the modes ξ_5 and ξ_6 have charge-transfer character at the spiro moieties. Further, they have nonequal delocalization between the biphenyl parts in the central and peripheral spiro-bifluorenes. This can be seen in the plot of ξ_5 where off-diagonal blocks have no counterparts at the opposite side of the diagonal. Similar intra-branch charge transfer properties are observed for CEO modes ξ_8, ξ_9, and ξ_{10} on all peripheral spiro-bifluorenes. These high frequency modes are localized mostly on the terminal edges, while the lower energy modes (ξ_5, ξ_6) are distributed around the main central spiro-linkage.

5. Conclusion

The synthesis of new optical materials for technological applications requires good physical and chemical knowledge of the mechanisms controlling the molecular optical response to an external field. The used CEO approach offers a unified and unique description of the real-space connection between the optical response and charge delocalization/localization in the molecule upon excitation. By displaying the ground-state one-electron density matrix $\bar{\rho}$ and the CEO eigenmodes ξ_ν in two-dimensional surface plots, a direct real-space connection between the linear optical response and spatial redistribution dynamics of the electronic probability amplitude upon excitation can be established very effectively. We conclude that the higher CEO modes (ξ_n, $n \geq 3$) with significant oscillator strengths mostly correspond to different spiro-centers, intra-branch, and inter-branch neutral electronic delocalization. Intramolecular, central and peripheral spiro group localized charge transfers have been found, too. The comparison of diagonal and coherence

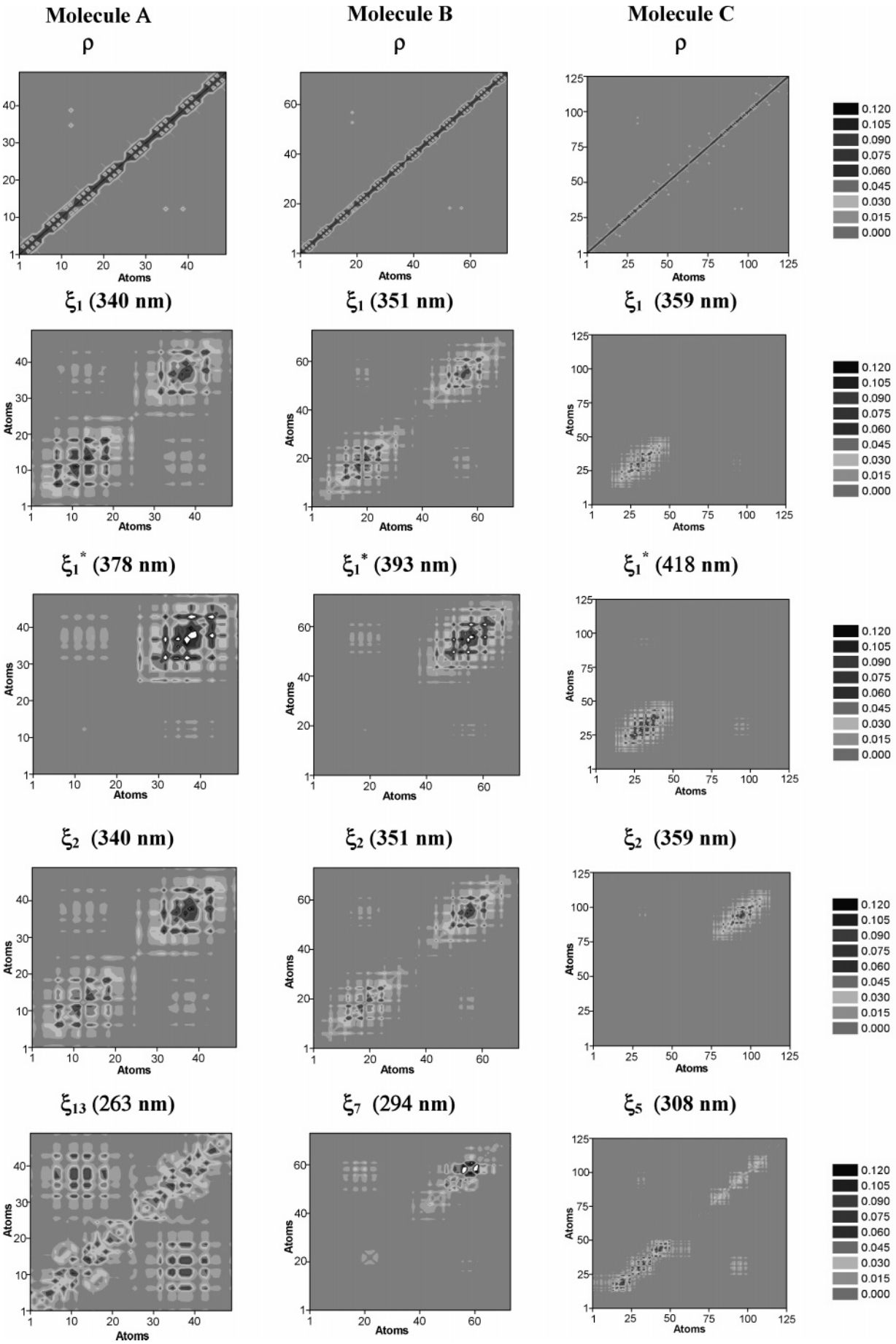
Molecule A
Molecule B
Molecule C
ρ
ρ
ρ
ξ1 (340 nm)
ξ1 (351 nm)
ξ1 (359 nm)
ξ1* (378 nm)
ξ1* (393 nm)
ξ1* (418 nm)
ξ2 (340 nm)
ξ2 (351 nm)
ξ2 (359 nm)
ξ13 (263 nm)
ξ7 (294 nm)
ξ5 (308 nm)
Atoms
0.120
0.105
0.090
0.075
0.060
0.045
0.030
0.015
0.000

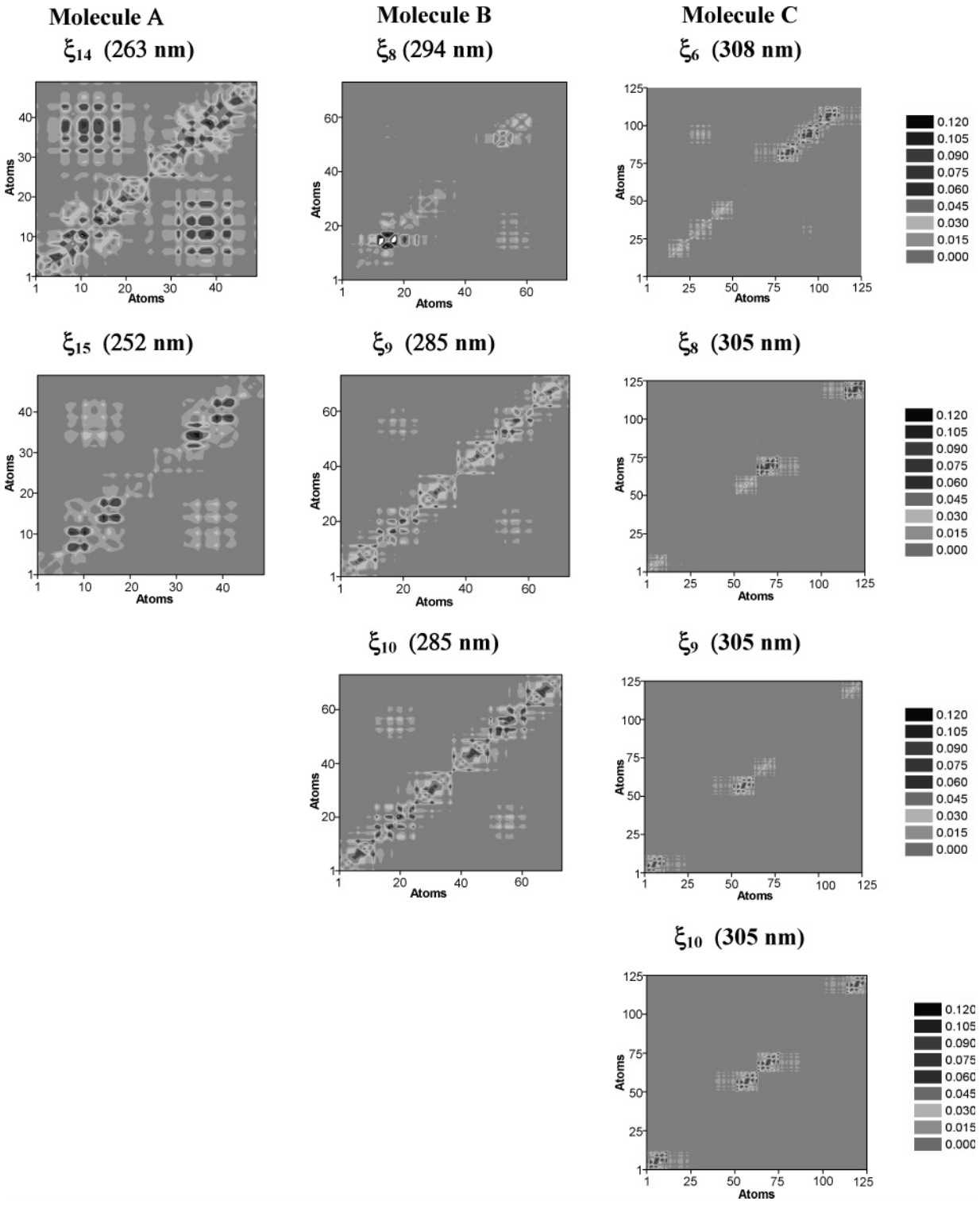

Figure 3. Surface plots of the ground-state density matrices, the first CEO modes and of related quantities in the ground (S_0) and lowest excited state (S_1) geometries of molecules **A**, **B** and **C**: ground-state density matrices $\bar{\rho}$ in S_0 geometry (first row); ξ_1 CEO modes in S_0 geometry (second row); ξ_1* CEO modes in S_1 geometry (third row); higher CEO modes with significant oscillator strengths in S_0 geometry (fourth to ninth rows).

lengths of the CEO modes of molecules **A** and **B** implies that the oligophenylene segment elongation supports electronic delocalization. Despite the same size of the oligophenyl moieties in **B** and **C**, the effect of peripheral spiro-linkages in **C** is overwhelming and reduces the charge delocalization to the level of molecule **A**. The adjacent spiro-linkages in molecule **C** induce intra-branch charge-transfer effects. Good agreement between the theoretical and experimental linear absorption and fluorescence data has been found. The presented results show that the length variation of central *p*-phenylene segments and the number of spiro-linkages can very sensitively modulate spectral properties. The electronic properties of these compounds can be relatively accurately predicted prior to synthesis using the semiempirical CEO approach.

Acknowledgment. The authors thank Prof. Salbeck and Dr. Fuhrmann for the synthesis of the studied compounds and Prof. Mukamel for the opportunity to perform calculations using the

CEO program package developed in his group. This work was supported by the Slovak Scientific Grant Agency (Projects No. 1/0055/03 and 1/2021/05) and funded within the framework of the Austrian Special Research Program ADLIS (F016, Austrian Science Foundation). J.S. gratefully acknowledges partial funding by the Doctoral Scholarship Program (DOC) of the Austrian Academy of Sciences.

References and Notes

(1) Prasad, P. N.; Williams, D. J. *Introduction to Nonlinear Optical Effects In Molecules and Polymers*; John Wiley: New York, 1991.

(2) André, J. M.; Delhalle, J.; Brédas, J. L. *Quantum Chemistry Aided Design of Organic Polymers. An Introduction to the Quantum Chemsitry of Polymers and its Applications*; World Scientific: Singapore, 1991.

(3) Mukamel, S. *Principles of Nonlinear Optical Spectroscopy*, Oxford University Press: New York; 1995.

(4) Bäuerle, P. In *Electronic Materials: The Oligomer Approach*; Müllen, K., Wegner, G., Eds.; Wiley−VCH: Weinheim, Germany, and New York, 1998; p 105.

(5) BolivarMarinez, L. E.; dosSantos, M. C.; Galvao, D. S. *J. Chem. Phys.* **1996**, *100*, 11029.

(6) Lupton, J. M.; Samuel, I. D. W.; Burn, P. L.; Mukamel, S. *J. Chem. Phys.* **2002**, *116*, 455.

(7) Karni, Y.; Jordens, S.; De Belder, G.; Hofkens, J.; Schweitzer, G.; De Schryver F. C. *J. Phys. Chem. B* **1999**, *103*, 9378.

(8) Salbeck, J.; Yu, N.; Bauer, J.; Weissörtel, F.; Bestgen, H. *Synth. Met.* **1997**, *91*, 209.

(9) DiCésare, N.; Belletête, M.; Marrano, C.; Leclerc, M.; Durocher, G. *J. Phys. Chem.* **1998**, *102*, 5142. 6.

(10) Cornil, J.; Beljonne, D.; Brédas, J. L. In *Electronic Materials: The Oligomer Approach*; Müllen, K., Wegner, G., Eds.; Wiley−VCH: Weinheim, Germany, and New York, 1998; p 432.

(11) Tsuzuki, S.; Uchimotu, T.; Matsumura, K.; Mikami, M.; Tanobe, K. *J. Chem. Phys.* **1999**, *110*, 2858.

(12) Guha, S.; Graupner, W.; Resel, R.; Chandrasekhar, M.; Glaser, R. Leising, G. *J. Phys. Chem.* **2001**, *A 105*, 6203.

(13) Shulz, M.; Tretiak, S.; Chernyak, V.; Mukamel, S. *J. Am. Chem. Soc.* **2000**, *122*, 452.

(14) Gigli, G.; Della Sala, F.; Lomascolo, M.; Anni, M.; Barbarella, G.; Di Carlo, A.; Lugli, P.; Cingolani, R. *Phys. Rev. Lett.* **2001**, *86*, 167.

(15) Pudzich, R.; Salbeck, J. *Synth. Met.* **2003**, *138*, 21.

(16) Johansson, N.; Salbeck, J.; Bauer, J.; Weissörtel, F.; Bröms, P.; Anderson, A.; Salaneck, W. R. *Adv. Mater.* **1998**, *10*, 1136.

(17) Milota, F.; Warmuth, Ch.; Tortschanoff, A.; Sperling, J.; Fuhrmann, T.; Salbeck, J.; Kauffmann, H. F. *Synth. Met.* **2001**, *121*, 1497.

(18) Milota, F. Diploma Work, University of Vienna, 2000.

(19) Steuber, F.; Staudigel, J.; Stössel, M.; Simmer, J.; Winnacker, A.; Spreitzer, H.; Weissörtel, F.; Salbeck, J. *Adv. Mater.* **2000**, *12*, 130.

(20) Johansson, N.; dos Santos, D. A.; Guo, S.; Cornil, J.; Fahlman, M.; Salbeck, J.; Schenk, H.; Arwin, H.; Brédas, J. L.; Salaneck, W. R. *J. Chem. Phys.* **1997**, *107*, 2542.

(21) Johansson, N.; Salbeck, J.; Bauer, J.; Weissörtel, F.; Bröms, P.; Andresson, A.; Salaneck, W. R. *Synth. Met.* **1999**, *101*, 405.

(22) Salbeck, J.; Schörner, M.; Fuhrmann, T. *Thin Solid Films* **2002**, *417*, 20.

(23) Lukeš, V.; Breza, M. *J. Mol. Struct.* **2004**, *699*, 93.

(24) Franco, I.; Tretiak, S.. *J. Am. Chem. Soc.* **2004**, *126*, 12130.

(25) Tretiak, S.; Mukamel, S. *Chem. Rev.* **2002**, *102*, 3171.

(26) Tretiak, S.; Zhang, W. M.; Chernyak, V.; Mukamel, *S. Proc. Natl. Acad. Sci. U.S.A.* **1999**, *96*, 13003.

(27) Tretiak, S.; Chernyak, *J. Chem. Phys.* **2003**, *119*, 8809.

(28) Tretiak, S.; Saxena, A.; Martin, R. L.; Bishop, A. R. *J. Phys. Chem. B* **2000**, *104*, 7029.

(29) Masunov, A.; Tretiak, S. *J. Phys. Chem. B* **2004**, *108*, 899.

(30) Zerner, M. C.; Loew, G. H.; Kirchner, R. F.; Mueller-Westerhoff, U. T. *J. Am. Chem. Soc.* **1980**, *102*, 589.

(31) Weisburger, J. H.; Weisburger, E. K.; Ray, F. E. *J. Am. Chem. Soc.* **1950**, *72*, 4250.

(32) Ahlrichs, R.; Bär, M.; Häser, M.; Horn, H.; Kölmel, C. *Chem. Phys. Lett.* **1989**, *162*, 165.

(33) CEO program package, Rochester, NY, 2000.

(34) Scherf, U.; List, E. J. W. *Adv. Mater.* **2002**, *14*, 477.

(35) Brandsen, B. H.; Joachain, C. J. *Physics of Atoms and Molecules;* Longman Group Limited: London, 1983.